



Bromide transport at a tile-drained field site: experiment, and one- and two-dimensional equilibrium and non-equilibrium numerical modeling

Sigrid Köhne^{a,b,*}, Bernd Lennartz^b, J. Maximilian Köhne^b, Jirka Šimůnek^a

^a*Department of Environmental Sciences, University of California, Riverside, 900 University Avenue, A135 Bourns Hall, Riverside, CA 92521, USA*

^b*Institute for Land Use, Faculty for Land use and Agricultural Sciences, University Rostock, Justus-von-Liebig-Weg 6, 18044 Rostock, Germany*

Received 7 October 2004; revised 6 August 2005; accepted 11 August 2005

Abstract

Systematically tile drained field sites have been recognized as one major source for surface water contamination with agrochemicals. To study the effects of tile drainage and physical non-equilibrium on solute transport in structured soil, bromide (Br^-) transport experiments were carried out on three plots (A, B, C) with different tile drain depths (128, 101, 96 cm) and spacings (16, 18 and 12 m) at the Infeld experimental field site (North–West Germany). Tile drain outflow along with Br^- concentrations were monitored over a half-year period. For all three plots, fast Br^- breakthrough was observed with Br^- concentrations fluctuating around levels below 6 mg/L during the experiment without a distinct concentration maximum. Experimental observations of plot B were analyzed using one-dimensional (1D) and two-dimensional (2D) single-porosity model (SPM) and mobile-immobile model (MIM) approaches. All SPM and MIM parameters were obtained from independent measurements, except for the calibrated MIM water and solute transfer coefficients. Water flow and Br^- transport were then predicted for the A and C plots using the model parameters as obtained for plot B. Measured plateau-like Br^- concentrations could only be consistently calibrated (plot B) and predicted (A and C) using the 2D-MIM approach, while the 1D-MIM, 2D-SPM, and 1D-SPM approaches (in this order) increasingly deviated from the experimental data. The MIM simulations suggested that solute transfer into the immobile region represented more than 60% of the surface applied Br^- . Non-equilibrium transport with advective and diffusive mass transfer increased early mass loss and entailed extended, slower leaching as compared to equilibrium transport. Furthermore, model simulations suggested that the two-dimensional flow field as induced by tile drains enhanced Br^- dispersion and accelerated Br^- appearance in the drain. This study showed that both

* Corresponding author. Address: Institute for Land Use, Faculty for Land use and Agricultural Sciences, University Rostock, Justus-von-Liebig-Weg 6, 18044 Rostock, Germany. Tel.: +1 979 779 3430.

E-mail addresses: sigrid.koehne@uni-rostock.de (S. Köhne), bernd.lennartz@uni-rostock.de (B. Lennartz), max.koehne@uni-rostock.de (J.M. Köhne), jiri.simunek@ucr.edu (J. Šimůnek).

the variably-saturated 2D flow field and physical non-equilibrium transport should be explicitly accounted for in physically based model simulations of solute transport in tile-drained structured field soils.

© 2005 Elsevier B.V. All rights reserved.

Keywords: Field-scale experiment; Subsurface-drainage; Physical non-equilibrium; Preferential flow and transport; Mobile-immobile model; two-dimensional modeling

1. Introduction

The loss of nutrients and pesticides from agricultural fields to subsurface drainage systems impairs ground and surface water quality (Richard and Steenhuis, 1988; Klavivko et al., 1991; Southwick et al., 1992). Physical non-equilibrium transport conditions initiated by preferential flow resulted into faster solute transport towards drains, and caused higher peak concentrations, than was expected under equilibrium conditions (e.g. Klavivko et al., 1991; Mohanty et al., 1998a,b; Lennartz et al., 1999; Gish et al., 2004). In this context, the term physical non-equilibrium is defined as local differences of water contents, pressure heads, and solute concentrations between bypasses (also denoted fractures, mobile or macropore regions/domains) and the soil matrix (Jarvis, 1998; Gerke and Van Genuchten, 1993). The extent of bypassing and physical non-equilibrium during flow and transport varies depending on various factors, such as soil water content, soil texture and structure, tillage, precipitation amount and intensity, and lag-time between solute application and rainfall (e.g. White, 1986; Bouma, 1990; Jaynes et al., 2001; Fortin et al., 2002).

Physically based numerical models are frequently used to analyze and predict solute transport in tile drained fields. Some models, for instance DRAIN-MOD (Skaggs, 1980) or SWMS_2D (Šimůnek et al., 1994), consider the drain-induced two-dimensional flow field, but are based on the single-porosity assumption, where water contents and pressure heads are always at local equilibrium. Such models were used by, among many others, Mohanty et al. (1998a,b) or Šimůnek and de Vos (1999) to simulate nitrate leaching from tile-drained fields. Other models relied on the dual-permeability concept to account for physical non-equilibrium transport, but were constrained to only one dimension (1D). For example, MACRO (Jarvis, 1994) was applied by Larsson and Jarvis (1998), Larsson et al. (1999), and Andreu et al.

(1994) to simulate physical non-equilibrium solute transport data from subsurface drained field plots. The 1D MACRO model approximates the effect of 2D saturated groundwater flow using a specific lower boundary condition. Recently, Kohler et al. (2001) developed and applied a 2D numerical dual-permeability model for analysis of preferential solute transport in tile-drained fields assuming 1D vertical flow in the macropore domain. There is still a lack of studies comparing 1D and 2D physical equilibrium and non-equilibrium models to systematically separate the spatial and preferential flow effects on solute transport at tile-drained field sites.

A common model for describing physical non-equilibrium solute transport in soils is the mobile-immobile model (MIM), also named dual-porosity model or two-region model (Van Genuchten and Wierenga, 1976). The MIM assumes that the soils' liquid phase is composed of a mobile region, in which transport is governed by convection and dispersion, and an immobile (stagnant) region. The two regions can exchange solutes by means of molecular diffusion. The MIM concept has recently been extended to consider transient, variably saturated water flow in the mobile region, and exchange of both water and solutes with the immobile region (Šimůnek et al., 2003). The MIM has the advantage of requiring considerably fewer parameters than the dual-permeability models with two interacting mobile regions (Gerke and Van Genuchten, 1993; Jarvis, 1994).

A variably saturated flow, simplified 1D MIM model with drain-boundary condition (an extension of the MACRO model) was used by Larsson et al. (1999) to analyze bromide transport data from a tile-drained field. Abbasi et al. (2004) applied a 2D MIM to analyze data from furrow irrigation experiments. However, the immobile water content was constant, preventing water transfer between mobile and immobile regions and allowing only for diffusive solute transfer between the regions (Abbasi et al., 2004). In this study, the MIM approach for variably

saturated flow and transfer of water and solute between the regions (Šimůnek et al., 2003) is extended to two dimensions and is implemented into the HYDRUS-2D model (Šimůnek et al., 1999).

The objective of this study was to investigate the effects of the tile-drain induced, two-dimensional flow field and of physical non-equilibrium on solute transport through a structured tile-drained soil. We approached our objective by first performing Br^- tracer tests on three plots with different tile drain spacing and depths at the Infeld tile-drained field site (Germany). These tests were then followed by the comparison of the experimental observations with simulation results obtained with one- and two-dimensional, single- and dual-porosity models.

2. Material and methods

2.1. The Infeld study site

The Infeld experimental station is located near Nordenham (Germany) in a Marsh-region that was systematically drained by open ditches and tile drains several decades ago. At the pasture cropped Infeld site, nutrient losses via tile drains have been monitored since 1975 by the county agricultural authority Landwirtschaftskammer Weser-Ems. The Infeld site (4.16 ha) is subdivided into 10 plots (0.1–0.24 ha) with different tile drain depths (79–130 cm) and spacings (10–18 m). At each plot, three tile-lines are routed to a measurement station. Plots are hydrologically isolated by surrounding discard drains, which are connected to the ditch system (see Fig. 1). Since 1975, drainage from the individual plots has been monitored continuously using tipping bucket samplers.

The soil at Infeld is a Fluvi-Dystric Gleysol according to FAO-classification. It was described in detail by Neuhaus (1983) and Diez and Weigelt (1987). Four main horizons were identified: H1 (0–25 cm depth), H2 (25–70 cm), H3 (70–135 cm), and H4 (135–200 cm). The H1 surface layer was characterized by subangular to crumb structure, whereas the subsoil layers showed angular to prismatic (H2) or dense prismatic (H3, H4) structure. The soil characteristics do not vary spatially over the experimental site. Soil texture as determined with a

combined sieve and sedimentation method (German Industrial Standard DIN 19683 T2) was very fine with more than 40% clay content in each horizon (Table 1). Additional soil properties are listed in Table 1.

In 1999, six undisturbed 250-cm³ samples were taken from each soil horizon by driving stainless steel cylinders vertically into the soil. Additionally, bulk soil material was collected. Water retention curves were measured by stepwise desaturation at 30, 50, 100, 150, 200, 300 and 600 cm suctions and in a pressure chamber at 15000 cm. The soil hydraulic van Genuchten's (1980) parameters α , n , and the saturated water content, θ_s , were estimated from the retention data using the RETC program (van Genuchten et al., 1991). The residual water content, θ_r , was fixed at 60% of the average water content of a particular soil horizon as measured in the pressure chamber (at 15000 cm). Additionally, the bulk density of each soil horizon was calculated as the arithmetic average of dry soil weights divided by sample volumes (Table 1).

Saturated hydraulic conductivities, K_s , of H1 and H2 were determined using the volume samples and a falling head permeameter. To determine the depth-averaged saturated hydraulic conductivity of the (combined H3 and H4) subsurface layers, the auger hole method according to Hooghout and Ernst (Twitty and Rice, 2001) was applied at seven boreholes (230-cm depth, 8-cm diameter). During the measurement period, the hydrostatic groundwater level in seven holes was located in the third (H3) layer and during the auger hole tests was lowered into the fourth (H4) layer.

2.2. Bromide transport experiments

A bromide tracer experiment was carried out in the winter of 1999/2000 on the plots N2, N4 and N8 of the Infeld experimental station. The plots N2, N4, and N8 are renamed A, B, and C for simplification from here onwards. A solution carrying 65.5 g/L bromide (Br^-) as potassium bromide (KBr) was sprayed on November 22th 1999 onto each plot with a volume of 0.066 L/m². At the time of application, tile drainage had not started yet, and the water table was below the deepest drain level at Infeld of 1.30 m. Table 2 summarizes the most important characteristics of the experiment. Rainfall (Hellmann rain gauge at 1 m height), relative humidity, temperature, wind speed,

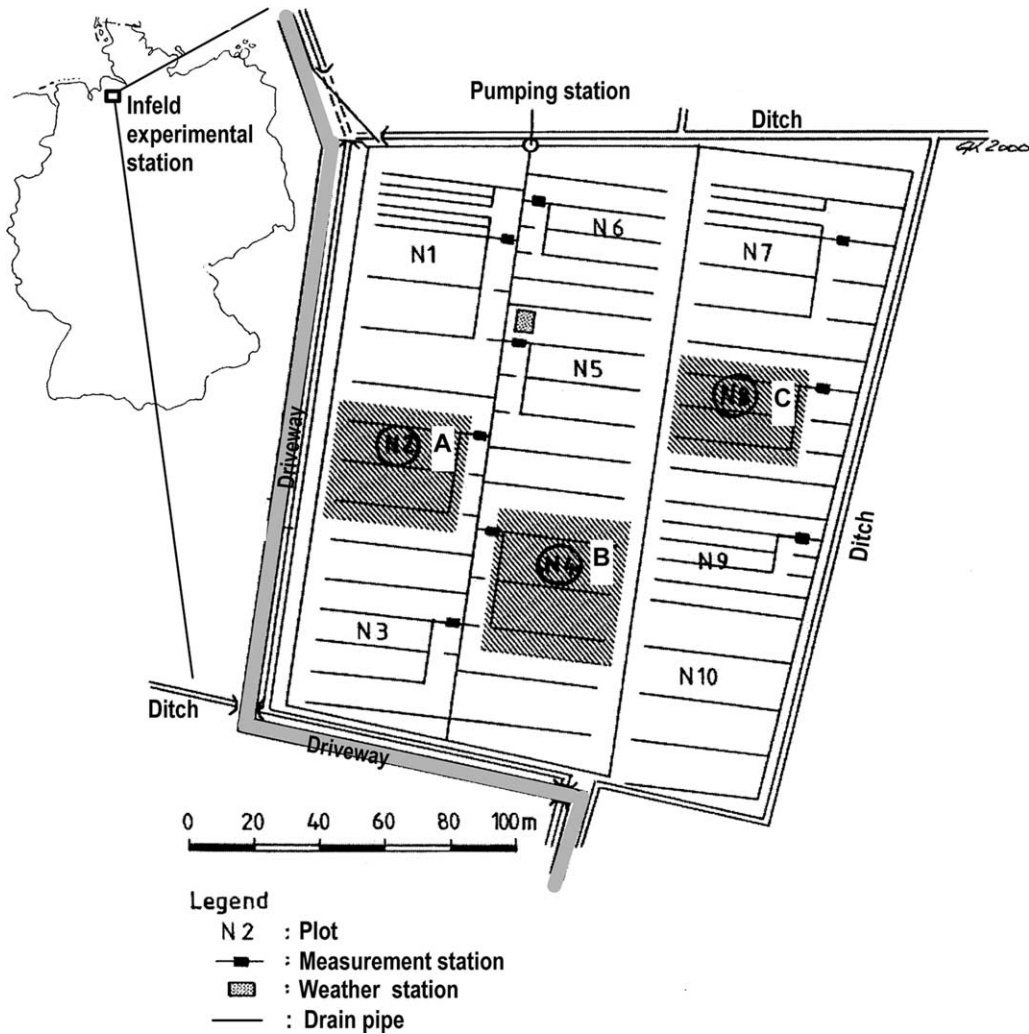


Fig. 1. Location of the Infeld experimental station in Germany and schematic view of the site.

and sunshine duration were measured daily. The rainfall data were corrected according to Richter (1995) to account for measurement errors caused by wind, evaporation and wetting of the Hellmann rain gauge. The potential evapotranspiration was calculated using the Turc-Wendling method (Wendling et al., 1991), while the actual evapotranspiration (ETA) was determined employing the soil water balance model of Wendling (DVWK, 1996). Fig. 2 shows the atmospheric conditions at the site during the experimental period. We note that the experiment was conducted in a relatively mild winter, for which

daily mean temperatures below 0°C were recorded only on 3 days (12/15/99, -0.3°C ; 1/10/00, -0.2°C ; 1/23/00, -1.8°C).

Drainage outflow (cm/d) was measured daily for plot A and every 6 h for plots B and C. Water samples of 90 cm^3 each were collected in 15-minute time intervals from the drainage effluent and were accumulated to 6-hour samples. The 6-hour samples were analyzed for Br^- concentration at the B and C plots, whereas for the A plot, four (6-hour) samples of a particular day were mixed to yield daily samples of Br^- concentrations.

Table 1
Selected soil properties at Infeld experimental site.

Horizon	Clay (%)	Silt (%)	Sand (%)	C _{org} (%)	Bulk density (g cm ⁻³)	pH (–)
H1	42.9	47.4	10.0	4.6	1.35	5.9
H2	57.4	38.7	4.3	0.9	1.31	6.8
H3	50.8	45.2	3.6	0.9	1.09	6.9
H4	43.7	53.1	1.1	n.d.	0.91	n.d.

Equivalent diameter of Clay, 0–0.002 mm; Silt, >0.002–0.063 mm; Sand, 0.063–2 mm. C_{org}, organic carbon. n.d., not determined.

Bromide was analyzed using a Metrohm Ion Chromatography system with a conductivity detector and chemical suppression. Anions were separated on a Metrosep Dual 2 column (75 × 4.6 mm; Metrohm, Switzerland). The flow rate of the mobile phase—a 1.3 mmol/L Na₂CO₃ and 2 mmol/L NaHCO₃ solution—was adjusted at 0.8 mL/min. Sample volume was 20 µL. The detection limit for Bromide was 0.15 mg/L.

2.3. Model description

Four different numerical model approaches were compared to describe and interpret the experimental observations: (i) one-dimensional single-porosity model (1D-SPM), (ii) one-dimensional dual-porosity mobile-immobile model (1D-MIM), (iii) two-dimensional single-porosity model (2D-SPM), and (iv) two-dimensional dual-porosity mobile-immobile model (2D-MIM). An extended version of HYDRUS-1D (Šimůnek et al., 1998, 2003) was used for 1D-SPM and 1D-MIM simulations, while similarly modified HYDRUS-2D (Šimůnek et al., 1999) was used for 2D-SPM and 2D-MIM simulations.

In the one-dimensional single-porosity model (1D-SPM), vertical variably-saturated water flow and non-reactive solute transport in the soil was described using the Richards' and convection dispersion

equations, respectively:

$$\frac{\partial \theta}{\partial t} = \frac{\partial}{\partial z} \left[K(h) \left(\frac{\partial h}{\partial z} + 1 \right) \right] \quad (1)$$

$$\frac{\partial \theta c}{\partial t} = \frac{\partial}{\partial z} \left(\theta D \frac{\partial c}{\partial z} \right) - \frac{\partial q c}{\partial z} \quad (2)$$

where θ is the volumetric water content [L³L⁻³], h is the pressure head [L], z the vertical coordinate (positive upward) [L], t is time [T], $K(h)$ is the hydraulic conductivity function [LT⁻¹], c is the solute concentration [ML⁻³], q is the flux density [LT⁻¹], and D is the dispersion coefficient [L²T⁻¹] defined as:

$$\theta D = \lambda q + D_0 \theta \tau \quad (3a)$$

$$\tau = \frac{\theta^{7/3}}{\theta_s^2} \quad (3b)$$

where λ is the dispersivity [L], D_0 is the molecular diffusion coefficient [L²T⁻¹], τ is the tortuosity coefficient [–], evaluated according to Millington and Quirk (1961), and θ_s is the saturated water content.

The one-dimensional mobile-immobile model (1D-MIM) describes vertical variably-saturated water flow and non-reactive solute transport in a soil characterized by mainly two pore systems. The MIM

Table 2
Characteristics of the bromide tracer experiments (22 Nov 1999 to 29 Apr 2000) at plots A, B, and C of the Infeld experimental station

Plot	Drain spacing (m)	Drain depth (m)	Plot size (m ²)	Start drainage	Total rainfall (cm)	Total drainage (cm)	Applied Br ⁻ mass (kg/Plot; g/m ²)
A	16	1.28	2208	3 Dec 1999	47.7	34.2	9.50; 4.3
B	18	1.01	2430	6 Dec 1999	47.7	30.6	10.43; 4.3
C	12	0.96	1620	2 Dec 1999	47.7	31.5	6.95; 4.3

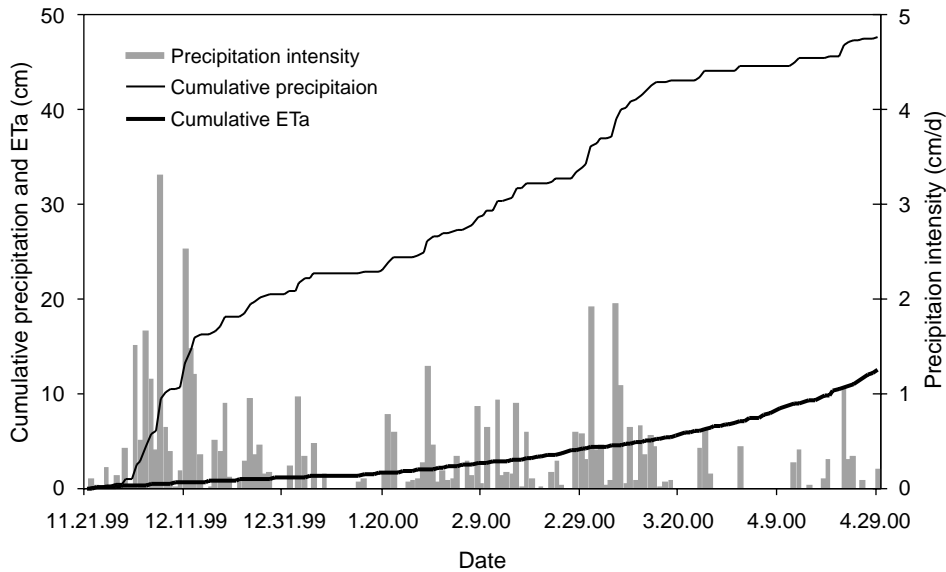


Fig. 2. Rain intensity, cumulative precipitation and actual evapotranspiration (ETa) at the Infeld experimental site during the tracer experiment (Nov. 21st 1999 to April 29th 2000).

assumes that the soil water content, θ , is partitioned into a mobile, θ_m , and an immobile, θ_{im} , fraction as follows:

$$\theta = \theta_m + \theta_{im} \tag{4}$$

This concept was incorporated into the Richards' (1) and convection-dispersion (2) equations as follows (e.g. Simunek et al., 2003):

$$\frac{\partial \theta_m}{\partial t} = \frac{\partial}{\partial z} \left[K_m(h) \left(\frac{\partial h_m}{\partial z} + 1 \right) \right] - \Gamma_w \tag{5a}$$

$$\frac{\partial \theta_{im}}{\partial t} = \Gamma_w \tag{5b}$$

$$\frac{\partial \theta_m c_m}{\partial t} = \frac{\partial}{\partial z} \left(\theta_m D_m \frac{\partial c_m}{\partial z} \right) - \frac{\partial q c_m}{\partial z} - \Gamma_s \tag{6a}$$

$$\frac{\partial \theta_{im} c_{im}}{\partial t} = \Gamma_s \tag{6b}$$

where indices m and im refer to the mobile and immobile regions, respectively. The rates of water and solute exchange between mobile and immobile regions, Γ_w [T^{-1}] and Γ_s [$ML^{-3}T^{-1}$], respectively, are described by the first-order terms (7) and (9).

Water exchange, Γ_w , was assumed to be proportional to the difference in relative saturations of the mobile and immobile regions:

$$\Gamma_w = \frac{\partial \theta_{im}}{\partial t} = \alpha_w [S_e^m - S_e^{im}] \tag{7}$$

where α_w is a first-order water transfer coefficient [T^{-1}], and S_e^m and S_e^{im} are the dimensionless effective saturations of the mobile and immobile regions given by

$$S_e^m = \frac{\theta_m - \theta_{m,r}}{\theta_{m,s} - \theta_{m,r}} \tag{8a}$$

$$S_e^{im} = \frac{\theta_{im} - \theta_{im,r}}{\theta_{im,s} - \theta_{im,r}} \tag{8b}$$

where $\theta_{m,s}$, $\theta_{m,r}$ ($\theta_{im,s}$, $\theta_{im,r}$) are the saturated and residual mobile (immobile) water contents [L^3L^{-3}], respectively.

The solute exchange term, Γ_s , includes diffusive (proportional to the concentration gradient between the mobile and immobile regions) and convective (proportional to water transfer and, depending on the direction of water transfer, the concentration in either mobile or immobile region) components as

follows:

$$\Gamma_s = \alpha_s [c_m - c_{im}] + \begin{cases} \Gamma_w c_m, & \text{if } \Gamma_w > 0 \\ \Gamma_w c_{im}, & \text{if } \Gamma_w < 0 \end{cases} \quad (9)$$

where α_s represents a first-order solute transfer coefficient [T^{-1}].

In the two-dimensional single-porosity model (2D-SPM), variably-saturated water flow and non-reactive solute transport in a two-dimensional vertical cross-section of the soil is described with the following forms of Richards' and convection dispersion equations:

$$\frac{\partial \theta}{\partial t} = \nabla [K(h) \nabla h] + \frac{\partial K(h)}{\partial z} \quad (10)$$

$$\frac{\partial \theta c}{\partial t} = \nabla [\theta D_{ij} \nabla c] - \nabla q c \quad (11)$$

where ∇ is the vector differential operator ($\partial/\partial x$, $\partial/\partial z$) and D_{ij} is the dispersion coefficient tensor [$L^2 T^{-1}$] evaluated according to Bear (1972) as

$$\theta D_{ij} = \lambda_T |q| \delta_{ij} + (\lambda_L - \lambda_T) \frac{q_j q_i}{|q|} + \theta D_0 \tau \delta_{ij} \quad (12)$$

where $|q|$ is the absolute value of the water flux [LT^{-1}], δ_{ij} is the Kronecker delta function ($\delta_{ij}=1$ if $i=j$, and $\delta_{ij}=0$ if $i \neq j$), λ_L and λ_T are the longitudinal and transverse dispersivities, respectively [L]. Eq. (10) assumes isotropic porous medium.

In the two-dimensional mobile-immobile model (2D-MIM), two-dimensional variably saturated water flow and physical non-equilibrium tracer transport in the soil with a secondary porosity was described by extending Eqs. (10) and (11) to yield:

$$\frac{\partial \theta_m}{\partial t} = \nabla \cdot [K_m(h_m) \nabla h_m] + \frac{\partial K_m(h_m)}{\partial z} - \Gamma_w \quad (13)$$

$$\frac{\partial \theta_{m,c_m}}{\partial t} = \nabla [\theta_m D_{ij} \nabla c_m] - \nabla q c_m - \Gamma_s \quad (14)$$

We note that in (14) the dispersion coefficient tensor, D_{ij} , is assigned to the mobile region. Furthermore, the relationships between θ , h , and K , or θ_m , h_m and K_m were defined by the van Genuchten-Mualem's functions (Van Genuchten, 1980) for both the single- and dual-porosity (i.e. mobile-immobile) models.

2.4. Modeling strategy

The basic idea was to first evaluate various one- and two-dimensional models with respect to their ability to describe the observations of tile drain outflow fluxes, cumulative tile drainage water flow, and Br^- concentrations in drainage water at the B plot, and then to use these model parameters to predict respective observations collected at the two other plots (A and C) with different drainage systems. Using the model approaches as described in Section 2.3, five different model cases were distinguished as follows: The 1D-SPM case and the 2D-SPM case used parameters that were either independently derived or fixed at estimated (not calibrated) values. The 1D- and 2D-MIM cases relied on inverse (1D) or 'semi-inverse' (2D) estimation of the transfer parameters α_w and α_s based on the experimental data collected at plot B. Finally, the 1D-MIMforward case used the transfer parameters of the 2D-MIM case. Procedures for estimating the input model parameters are described in the sections below.

Water flow and Br^- transport observations of the plots A and C were then predicted using the 2D-MIM, the 1D-MIM, and the 1D-MIMforward cases.

2.5. Model parameters

Input parameters for various models are presented in Table 3. All 1D- and 2D-SPM parameters were independently derived or were fixed at estimated (not calibrated) values. Water retention and hydraulic conductivity parameters were estimated from measured laboratory and field data as described above in Section 2.1. The dispersivity was set to 0.5 cm, a value in the range of laboratory observations obtained with undisturbed columns (Meyer-Windel, 1998; Maraqa et al., 1997).

Based on the range of values for the fraction of mobile water in field soils or large undisturbed soil columns as reported in Vanderborght et al. (1997), and considering the Infeld soil profile as well as using Eq. (4), mobile and immobile water contents, $\theta_{m,s}$ and $\theta_{im,s}$, for the MIM model were roughly estimated. For the top (H1) layer with a dense network of subangular to crumb structure, half of the total saturated water content was assigned to both mobile ($\theta_{m,s}=0.5\theta_s$) and immobile ($\theta_{im,s}=0.5\theta_s$) regions. To represent more

distinct interaggregate flow path regions of the (H2, H3, and H4) subsoil layers with angular to prismatic structure, a smaller fraction of θ_s was assumed to be mobile (i.e. $\theta_{m,s}=0.2\theta_s$), while the remaining fraction was assumed to be immobile (i.e. $\theta_{im,s}=0.8\theta_s$). The residual water content of the mobile region, $\theta_{m,r}$, was assumed to be zero.

The three different modeling cases for the mobile immobile model differed with respect to the treatment of the solute and water transfer parameters: (i) 2D-MIM case: The transfer parameters α_w and α_s of the H1–H4 layers for the 2D-MIM approach were estimated from the observations of plot B using a combined inverse analysis and subsequent manual ‘fine-tuning’ calibration. To reduce the number of fitted parameters from 8 (4 layers) to 6, α_w and α_s were constrained to similar values in the lower two layers (i.e. $\alpha_w(\text{H3})=\alpha_w(\text{H4})$ and $\alpha_s(\text{H3})=\alpha_s(\text{H4})$), which was consistent with the assumption of a single K_s value and with the observation of relatively similar structure in the H3 and H4 layers. (ii) 1D-MIM case: We attempted to fit the 1D-MIM water and solute transfer parameters, α_w and α_s , similarly as done for the 2D-MIM, in order to evaluate the capacity of the 1D-MIM for the best possible representation of the data, and to compare corresponding fitted 1D-MIM and 2D-MIM parameters. However, the simultaneous optimization of α_w and α_s in the 1D-MIM failed (i.e. led to program abortion). Alternatively, we inversely estimated α_s while keeping the previously (2D-MIM) obtained α_w values. (iii) 1D-MIMforward: both α_w and α_s were used as obtained with the 2D-MIM case.

For the inverse parameter identification in the 1D- and 2D-MIM approaches, the Levenberg-Marquardt optimization algorithm was used to minimize the weighted squared deviations between observations and simulated values (Simunek et al., 1999):

$$\Phi(\mathbf{b}) = \sum_{j=1}^m v_j \sum_{i=1}^n w_{i,j} [O_j(z, t_i) - E_j(z, t_i, \mathbf{b})]^2 \quad (15)$$

where m is the number of different sets of measurements (cumulative drainage, drainage rates, and Br^- concentrations of the tile-drain effluent), n represents the number of observations in a particular measurement set, $O_j(z, t_i)$ are observations at time t_i at location z , $E_j(z, t_i, \mathbf{b})$ are the corresponding estimated space-time variables for the vector \mathbf{b} of optimized

parameters and v_j and $w_{i,j}$ are weighting factors associated with a particular measurement set or point, respectively. In the 1D-MIM (2D-MIM) optimization, the vector \mathbf{b} consisted of α_s (α_w and α_s) for the three (4) soil horizons. Furthermore, we assumed that the weighting coefficients $w_{i,j}$ in (15) were equal to one, which is similar to assuming equal variances of the errors within a particular measurement set.

2.6. Initial and boundary conditions

Initial soil moistures and pressure heads were not known, but were fixed to represent a field capacity type moisture profile based on following considerations. Since drainage flow stopped on July 10, 1999, and did not start since, the groundwater table was certainly well below the tile drain level. On the other hand, repeated rainfall (15.2 cm since mid September 1999) prevented the soil from drying out. The initial condition for water flow was set to a linear pressure head increase between -600 h Pa at the upper boundary ($\theta(-600 \text{ h Pa})=0.468$ for $\theta_s=0.509$) and -100 h Pa at a 200-cm depth ($\theta(-100 \text{ h Pa})=0.634$ for $\theta_s=0.640$). Initial Br^- concentrations in the soil were assumed to be zero.

Daily values of rainfall and actual evapotranspiration were used as the upper boundary condition for water flow. The flux (Neumann) condition automatically changed into a prescribed ponding head (Dirichlet) boundary condition when a ponding depth of 0.2 cm was reached. When the calculated flux became less than the prescribed flux, the prescribed head (ponding of 0.2 cm) boundary condition switched back to the prescribed flux. During ponding, the difference between calculated and prescribed flux was considered to be surface runoff (overland flow). Zero flux boundary conditions were imposed for both vertical sides and the lower boundary of the 2D domain. A third-type (Cauchy) boundary condition was used for the solute condition.

The lower boundary condition for 1D simulations represented groundwater flow towards drains as calculated according to the Hooghoudt equation (e.g. Simunek et al., 1998). The drain parameters, i.e. the entrance resistance and the wet perimeter were set to 5 and 25 cm, respectively; the drainage geometry (drain spacing and depth) was specified according to plot characteristics (Table 2), and the

saturated hydraulic conductivity, K_s , in the Hooghoudt equation was calculated from the borehole method (see above).

In two-dimensional simulations the drain pipe was represented by a system-dependent water flow boundary condition at a single node that switched between zero flux for an unsaturated drain node to a zero pressure head upon saturation. To represent the entrance resistance of the drain, the hydraulic conductivities at the nodes adjacent to the drain node were reduced according to the method of Fipps and Skaggs (1986). An effective drain diameter of 4 cm was assumed and the standard correction factor (Fipps and Skaggs, 1986) was applied without additional reduction factor. A zero gradient (Neumann) boundary condition was assumed for solute transport out of the tile drain.

2.6.1. Numerical Grids

The size of the transport domain for one-dimensional simulations was set equal to the corresponding tile depth (127 cm for plot A, 101 cm for B, and 96 cm for C). Each domain was subdivided into 101 nodes at regular vertical increments.

The depths of the transport domain for two-dimensional simulations was set equal to the vertical tile location plus 100 cm, in order to minimize the effect of the lower impermeable boundary. The domain width was equal to the half-distance between drains. Resulting transport domains were subdivided into 46 (A), 51 (B), and 35 (C) vertical columns, and 49 (A) or 44 (B, C) horizontal rows at variable spacing with higher spatial resolutions at layer interfaces and near the drain node. The model drain node was located at one side of the transport domain at 128 (101, 96) cm depth for plot A (B, C). The domain was subdivided into four horizontal layers representing H1–H4 as described in Table 2.

3. Results and discussion

3.1. Experimental data and simulation results for plot B

Outflow from the plot B tile lines started on December 6th 1999 and the cumulative drainage was equal to 30.6 cm (64% of the rainfall) over the

duration of the experiment (Table 2). Fig. 3 compares the observed cumulative drainage (Fig. 3a) and drainage rates (Fig. 3b, c) from plot B with the one- and two-dimensional single-porosity model (SPM) and mobile-immobile model (MIM) cases. The measured cumulative drainage (Fig. 3a) was matched closely by the 2D-SPM and 2D-MIM cases. Cumulative drainage tended to be overestimated by both 1D-cases in the beginning but was underestimated and matched by the 1D-SPM and the 1D-MIM, respectively, in the end. Measured drainage rates reached maxima of about 1.9 cm/d, but frequently dropped below 0.5 cm/d. Both 2D models, i.e. 2D-SPM and 2D-MIM, matched the drainage rate peaks above 1 cm/d considerably better than the corresponding 1D models (compare Fig. 3b and c).

Bromide concentration data and model simulation results are compared in Fig. 4. Measured Br^- concentrations in the tile drainage effluent fluctuated around a value of 5 mg/L throughout the experiment (Fig. 4a), without obvious reactions to variations in tile-drain discharge. Bromide was found in the effluent from the start of drainage onward. By contrast, the 2D-SPM simulated the first appearance of Br^- in the drain to occur 1 month (or 10 cm of drainage) later, and the 1D-SPM simulation even gave a 2.5-month (or about 20 cm of drainage) time-lag between application and Br^- arrival in drain discharge (Fig. 4a). Accordingly, both SPM models underestimated the Br^- mass recovery in drain effluent at the end of the drainage period: the simulations suggested recoveries of 2.5% (1D-SPM) and 8.6% (2D-SPM) as compared to the 25% actually retrieved in the field experiment (Table 4). Similar to the measurements, the 2D-SPM simulation showed short term fluctuations of the Br concentrations whereas the 1D-SPM simulated BTC was smooth (Fig. 4a).

Fig. 4b compares measured Br^- BTCs with those simulated using 1D and 2D dual-porosity models. The 2D-MIM matched the measured Br^- concentrations very well in terms of the first appearance of Br^- , the concentration level and the short-term fluctuation pattern. The 1D-MIM forward case (using 2D-MIM fitted transfer parameters) predicted a 1 week (or 5 cm of drainage) delayed arrival and slow increase of Br^- concentrations, while it overestimated Br^- concentrations in the last third of the experiment. The 1D-

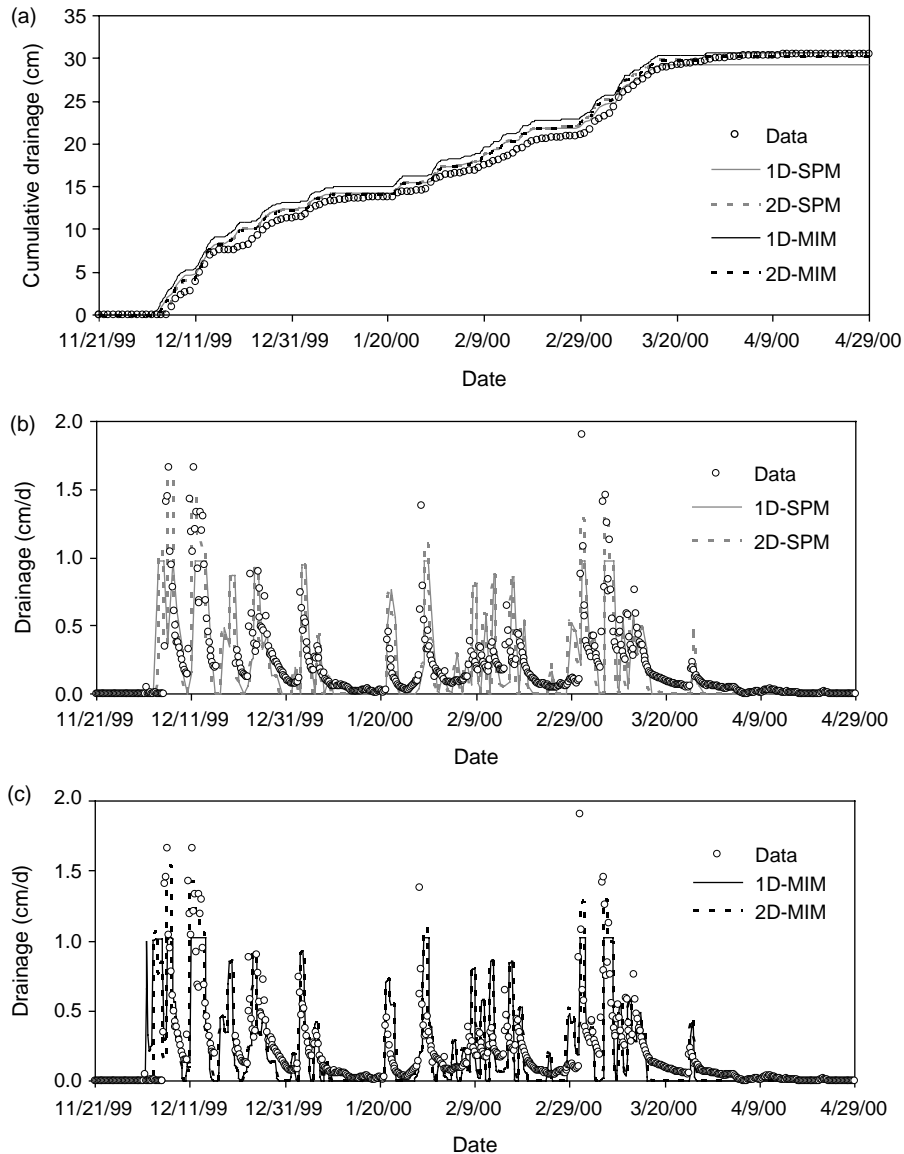


Fig. 3. Time series of drainage data, and one- and two-dimensional single-porosity model (SPM) and mobile-immobile model (MIM) results for plot B (18 m drain spacing, 1.01 cm drainage depth): a) cumulative drainage, b) drainage data and SPM results, and c) drainage data and MIM results.

MIM case (with fitted α_s , solid, thin line in Fig. 4b) gave slightly better simulation results than the 1D-MIMforward case.

The effect of using a 2D model vs. a 1D model on the simulation results is discussed in the following. The BTC simulated with the two-dimensional models (both SPM and MIM) started earlier and better

represented the observed concentration fluctuations than the corresponding 1D cases. This can be explained as follows: in the two-dimensional flow field, solute is transported along different pathways in terms of path lengths, orientations and water saturations. Directly above the drain, Br^- travel distance is shortest and is oriented vertically towards

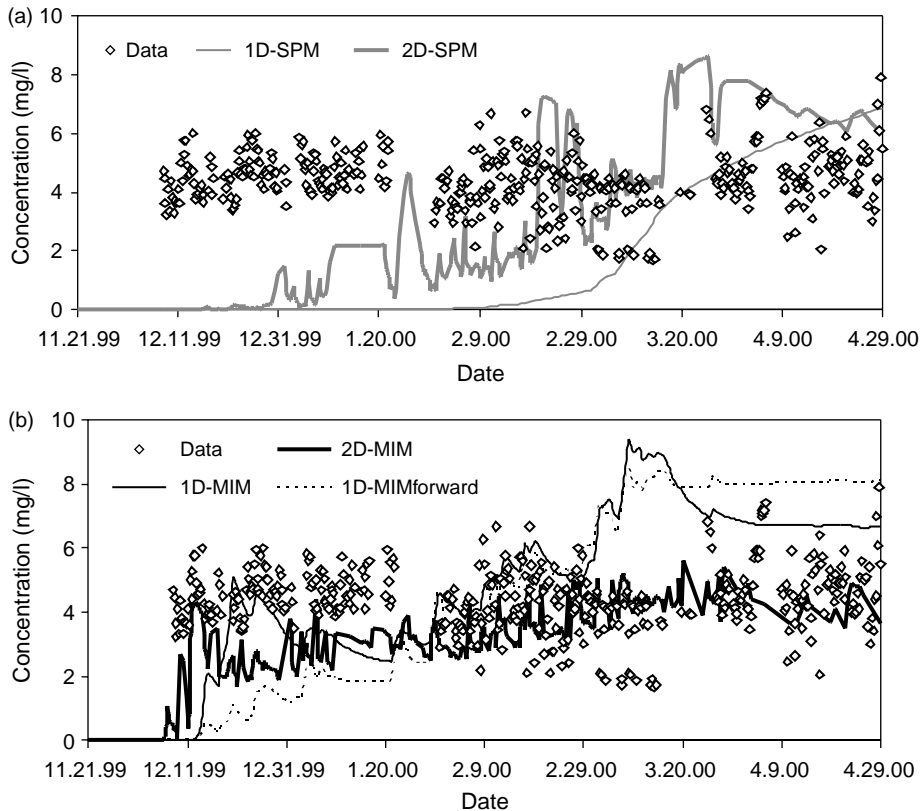


Fig. 4. Measured bromide concentrations, and one- and two -dimension single-porosity model (SPM) and mobile-immobile model (MIM) results for plot B (18 m drain spacing, 1.01 cm drainage depth): a) data and SPM results, b) data and MIM results.

the drain. At half drain-spacing, the total transport distance was largest, with mainly vertical orientation but shorter path length through the unsaturated zone, followed by a predominantly lateral (curved) flow paths in groundwater towards the drain. This variation in transport path lengths, directions and velocities in unsaturated zone and groundwater enhanced mixing of Br^- with a larger soil water volume and caused early arrival, dispersion, and fluctuation of simulated Br^- concentrations at the tile drain, similar to the field observations.

The additional effect of considering dual-porosity vs. equilibrium models becomes obvious by the fact that the simulation results of all MIM cases were closer to the measured Br^- concentrations than both 1D- and 2D-SPM cases (Fig. 4a,b). Accordingly, MIM-simulated Br^- mass losses were much closer to the observed loss (Table 4). The improvement yielded

with dual-porosity over single-porosity models to reproduce the observed rapid solute breakthrough and higher total solute losses was found earlier and was explained with preferential flow in structured soils (e.g. Larsson and Jarvis, 1999; Haws et al., 2005).

However, for surface-applied solutes, preferential flow conditions were typically associated with the highest concentration peak occurring after the first major rainfall event following solute application (e.g. Kladvik et al., 1991; Jardine et al., 1993; Lennartz et al., 1999; Gerke and Köhne, 2004; Gish et al., 2004), a close correspondence between concentration peaks and outflow peaks (Lennartz et al., 1999; Kung et al., 2000; Jaynes et al., 2001; Kohler et al., 2003) and high tracer recoveries in tile drain discharge amounting to at least 40–60% of the applied mass at the end of the drainage season (e.g. Lennartz et al., 1999; Köhne and Gerke, 2005). The BTC as observed

at the Infeld site lacked most of these preferential flow characteristics, except for the early solute arrival. In this context, Skaggs et al. (1998) and Kohler et al. (2003) stated that at tile drained fields, transport through the saturated zone may effectively remove any concentration pattern of preferential transport. However, this cannot be true for all tile drained fields, where preferential solute breakthrough in tile drainage effluent was often observed, as found in many of the studies mentioned above. Utermann et al. (1990) showed for simulations of solute transport towards a drain using a bimodal probability density function approach for the unsaturated zone and a streamline model for the saturated zone, that the bimodal concentration distribution simulated in the vadose zone developed lower and wider peaks after passage through the saturated zone. Yet similar to our results, in the simulations of Utermann et al. (1990) the early first appearance of a tracer as caused by preferential flow was not retarded by transport through the saturated zone.

Based on our 2D-MIM simulation results, the main mechanism leading to the weakly preferential BTC characteristics at the Infeld site is large mobile-immobile solute transfer, which will be discussed in the following. Fig. 5 shows the dual-porosity simulated (1D-MIM, 1D-MIMforward, 2D-MIM) relative Br^- mass in the immobile region (as a fraction of the applied mass) over time. All MIM approaches simulated an initially increasing immobilization of surface-applied Br^- , showed a slight inflection at the onset of tile outflow, and a continued rise until December 15th 1999, when approximately

67% of the applied Br^- mass was immobilized. Only after heavy rainfall and increased drainage rates in the first week of March 2000 did the Br^- net mass in the immobile region gradually decrease, but it remained above 60% throughout the drainage season. For comparison, Meyer-Windel (1999) found in Br^- transport experiments with structured soil columns subject to transient water flow conditions that 20 to 60% of the applied Br^- mass was immobilized in the soil after the Br^- concentrations in the effluent decreased to values below the detection limit. Obviously, solute release from immobile into mobile regions is very slow as compared to the solute transfer from mobile into immobile regions. For a surface applied tracer, fast net immobilization may be caused by high-rate advective transfer during initial infiltration, where differences in saturation between mobile and immobile regions are higher. Relatively large fitted α_w values suggest that this was a major mechanism for the two upper layers. Likewise, diffusive mass transfer is intensified due to high concentration gradients since the solute is entering the soil via the mobile region only, whereas the immobile regions are initially solute free. The backward process is taking place at a smaller rate, since on one hand concentration gradients are less steep (both regions carry solute), and on the other hand, with each new infiltration cycle following redistribution, advective transport from mobile to immobile regions is reiterated. Our model results suggest that relatively large solute transfer into the immobile regions restrained preferential solute transport by reducing the initial Br^- peak and overall Br^- loss. Inter-region

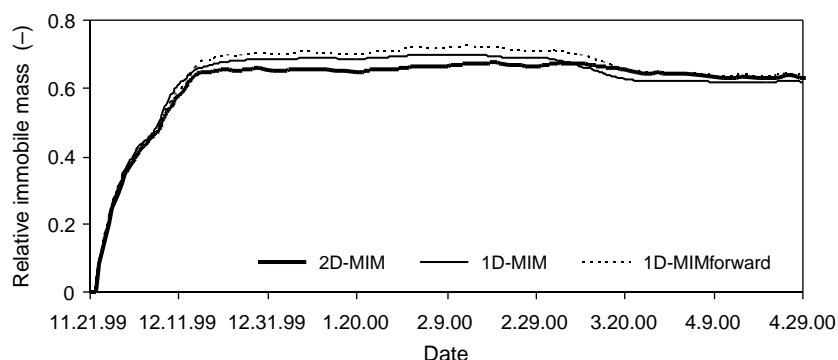


Fig. 5. Time series' of the relative bromide mass in the immobile region (fraction of the applied mass) of the soil profile as calculated using one- and two-dimensional mobile-immobile models (1D-MIM and 2D-MIM, respectively).

Table 3
Soil hydraulic parameters for the one- and two-dimensional single- and dual-porosity model simulations

Horizon	Depth (cm)	θ_s ($\text{m}^3 \text{m}^{-3}$)	θ_r ($\text{m}^3 \text{m}^{-3}$)	α (cm^{-1})	n	K_s (cm d^{-1})	θ_{ms} ($\text{m}^3 \text{m}^{-3}$)	θ_{mr} ($\text{m}^3 \text{m}^{-3}$)	θ_{ims} ($\text{m}^3 \text{m}^{-3}$)	θ_{imr} ($\text{m}^3 \text{m}^{-3}$)	α_w (d^{-1})	α_s (d^{-1})
H1	0–25	0.509	0.19	0.0010	1.59	4.8	0.254	0	0.254	0.190	0.12 ^a	0.020 ^a 0.020 ^b
H2	25–70	0.541	0.20	0.0008	1.39	14.9	0.108	0	0.433	0.200	0.10 ^a	0.021 ^a 0.023 ^b
H3	70–135	0.576	0.18	0.0010	1.53	35.0	0.115	0	0.460	0.180	0.07 ^a	0.075 ^a 0.016 ^b
H4	135–200 ^c	0.640	0.21	0.0014	1.67	35.0	0.128	0	0.512	0.210	0.07 ^a	0.075 ^a

Following transport parameters were assumed to be identical in all model simulation: dispersivity: $\lambda = 0.5$ cm; the effective bromide diffusion coefficient: $D_0 = 1.797 \text{ cm}^2 \text{ d}^{-1}$

^a Fitted with 2D-MIM and B data.

^b Fitted with 1D-MIM and B data.

^c 135–230 for simulations of plot A.

mass transfer and lateral mixing have been identified previously as a major factor controlling preferential solute transport (e.g. Flüher et al. 1996). Jaynes et al. (2001) and Fortin et al. (2002) suggested that mobile-immobile solute transfer may considerably reduce leaching losses.

Here, relatively large values for the first-order rate coefficient for water transfer, α_w , controlling advective solute transfer, were obtained between 0.12 and 0.07 d^{-1} for top and subsoil layers, respectively (Table 3). For simulations of field-scale preferential flow and solute transport, α_w values were found which were within similar range (Köhne and Gerke, 2005), or smaller, i.e. around 0.02 d^{-1} (Gerke and Köhne, 2004) or even below 0.004 d^{-1} (Haws et al., 2005) when pronounced preferential flow conditions prevailed. On the other hand, values for the solute transfer rate coefficient, α_s , between 0.02 and 0.07 d^{-1} for top and subsoil layers were within the range of 10^{-3} to 10^0 d^{-1} reported by others for physical non-equilibrium conditions (e.g. Jaynes et al., 1995; Lennartz and Meyer-Windel, 1995, Köhne and Gerke, 2005; Haws et al., 2005). Abbasi et al. (2004) obtained much higher α_s values in their furrow-irrigation field experiment with Bromide. Although variably saturated flow conditions prevailed in the experiment, the 2D MIM model used by Abbasi et al. (2004) did not consider advective solute transfer, such that their high α_s values accounted for advective and diffusive transfer in a lumped fashion.

The above model simulation results indicate that the plateau-like, preferential Br^- BTC at the Infeld tile drained site is a product of both, the two dimensional flow field and non-equilibrium transport characteristics with pronounced transfer between mobile and immobile regions. Additionally to the spreading of the BTC caused by the 2D flow field, the solute mass transfer from mobile to immobile regions has buffered concentrations at the tile drain, since solute has been taken out of the mobile flow regions.

Although pronounced solute mass transfer governed the tracer transport at Infeld, the simulated leaching loss during the 1999/2000 drainage season was still higher under the physical non-equilibrium transport conditions involving mass transfer (17%, 2D-MIM in Table 4) than under equilibrium conditions (8.6%, 2D-SPM in Table 4). To evaluate the effect of physical non-equilibrium transport and mass

Table 4
Observed and simulated bromide recovery (kg and (% of applied mass)) in drain outflow

Plot	Data	1D-SPM	2D-SPM	1D-MIM	2D-MIM
A	1.96 (20.6)	n.s.	n.s.	1.35 (14.3) ^a 0.81 (14.3) ^b	1.19 (12.5)
B	2.59 (24.8)	0.26 (2.5)	0.90 (8.6)	2.22 (21.3) ^a 1.86 (17.8) ^b	1.83 (17.5)
C	1.88 (27.0)	n.s.	n.s.	2.32 (33.4) ^a 2.71 (31.2) ^b	1.40 (20.1)

n.s., not simulated.

^a 1D-MIM case.

^b 1D-MIMforward case.

transfer on long term solute loss, we compared 2D-SPM and 2D-MIM model predictions of solute losses until the end of the year 2000 (no atmospheric data were available thereafter). These two model cases equally simulated a drainage depth of 6.6 cm for November/December 2000 (i.e. less than 25% of the drainage of the entire 1999/2000 drainage season). Fig. 6 shows the simulated relative Br^- mass losses until the end of 2000. About the same amount (8.4% of the applied mass) of Br^- as in the entire 1999/2000 drainage season (8.6%) is leached in the following half-season in the 2D-SPM equilibrium case. Although the total loss is higher in the 2D-MIM case assuming physical non-equilibrium and mass transfer, the leaching loss in the 2nd (half) drainage season is with 6% of the applied mass only one third of the 1999/2000 loss and is 2.5% less than that of the 2D-SPM case. This means that conservative solute leaching under physical non-equilibrium conditions

may in the long run proceed slower than for equilibrium or no-mass transfer conditions.

3.2. Predictions for different drainage systems (A and C plots)

Simulation results for the B plot showed that the dual-porosity concept represented Br^- transport observations at the Infeld site better than the single-porosity concept. As a next step, we applied the 1D- and 2D-MIMs with their plot B parameters to predict water flow and Br^- transport observations at the A and C plots, which differed from B with regard to drainage depths and spacing. The purpose of carrying out the MIM predictions was to further evaluate the importance of considering two dimensions in MIM by comparing how well the 1D- and 2D-MIM approaches can predict solute transport data at other plots with different drainage systems.

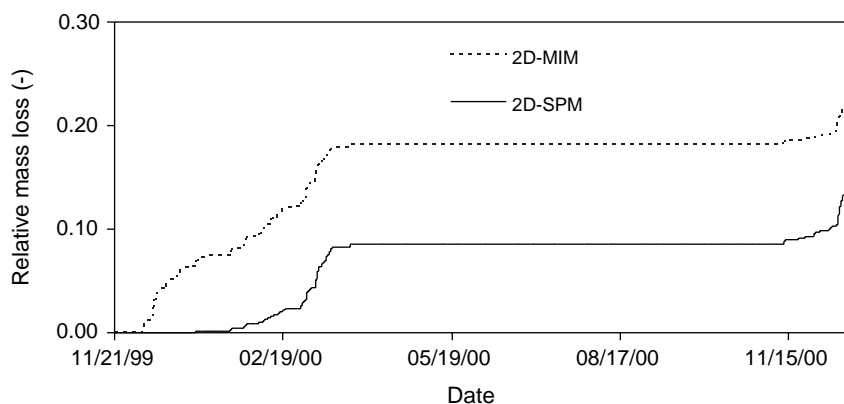


Fig. 6. Time series of relative cumulative bromide mass loss (fraction of applied mass) as simulated with two-dimensional mobile-immobile (2D-MIM) and single porosity (2D-SPM) models.

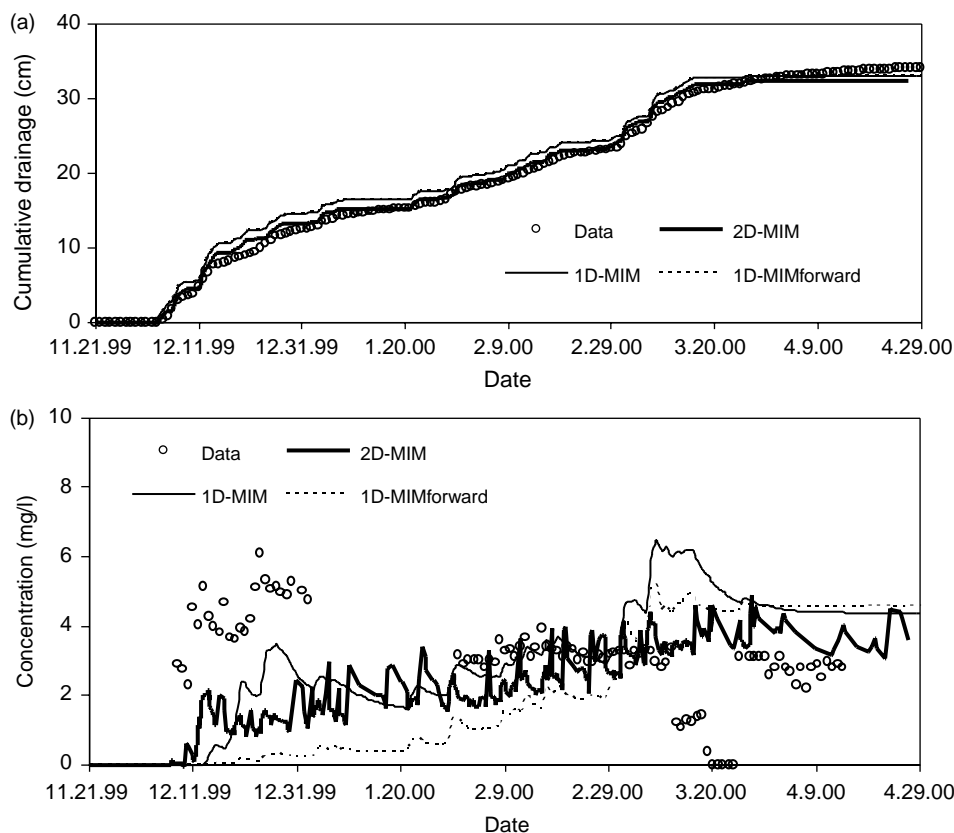


Fig. 7. Measured cumulative drainage (a) and bromide concentrations (b) compared with one- and two-dimensional mobile-immobile model (MIM) predictions for the plot A (16 m drain spacing, 128 cm drainage depth).

The A plot had a tile drainage system characterized by a considerably larger depth (128 cm) and somewhat narrower spacing (16 m) than the B plot (101 cm depth, 18 m spacing) (see Table 2). Fig. 7 compares the observed tile drain outflow and Br^- concentrations with one- and two-dimensional MIM predictions for the A plot. Compared with B, the drainage at A started 3 days earlier and yielded a 3.6 cm higher total value at the end of the experiment, which is consistent with the deeper tile-drain level (Fig. 7a, Table 2). The cumulative drainage was matched well by the 2D-MIM and was most of the time slightly overestimated by the 1D-MIM cases, similarly as for the B plot (compare Figs. 3a and 7a). As the soil hydraulic parameters were the same for both 1D-MIM and 1D-MIMforward, their simulated drain outflow curves were identical.

Measured Br^- concentrations quickly reached an initial level of 5–6 mg/L during December 1999 (Fig. 7b). After a month of missing data, observed Br^- concentrations fluctuated around a lower level of 3–4 mg/L, with a dip in concentrations in March 2000. Neither of the MIM predictions matched the Br^- concentration data very well (Fig. 7b). Simulated Br^- mass recoveries in drain effluent underestimated the measurement of the A experiment (Table 4). Still, the 2D-MIM was the best in predicting the onset of the observed Br^- concentrations and the later plateau-like shape of the Br^- BTC. The 1D-MIMforward (using water and solute transfer coefficients obtained for 2D-MIM for plot B) initially predicted a late appearance of Br^- in drainage and significantly underestimated Br^- concentrations. During the last third of the experiment,

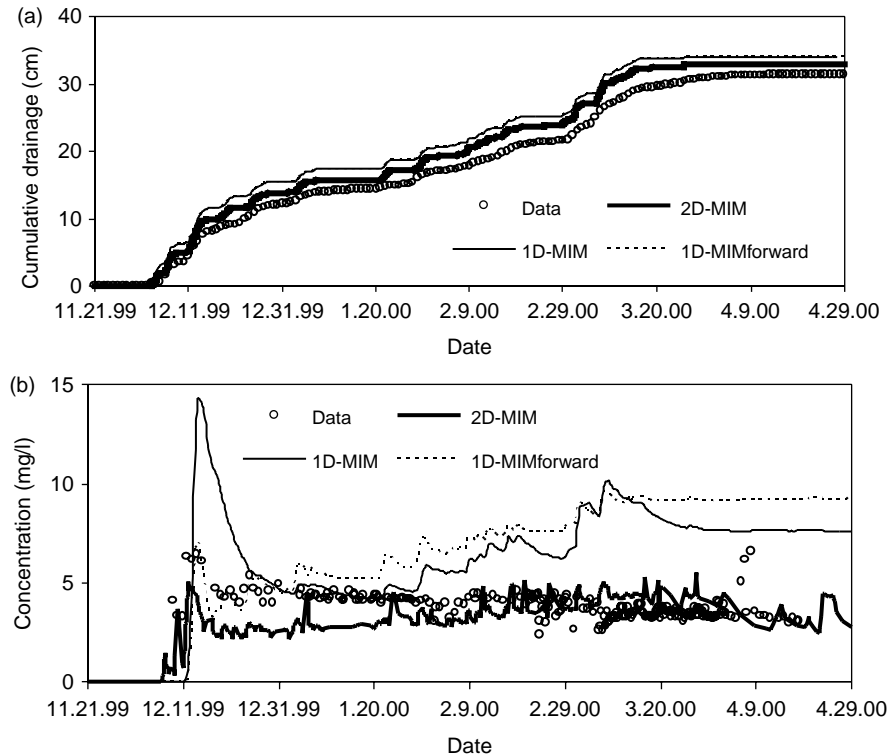


Fig. 8. Measured cumulative drainage (a) and bromide concentrations (b) compared with one- and two-dimensional mobile-immobile mode (MIM) predictions for the plot C (12 m drain spacing, 96 cm drainage depth).

the 1D-MIMforward predicted Br^- concentrations exceeding the measured values by about 2 mg/L (Fig. 7b). The Br^- BTC predicted with the 1D-MIM (with the solute transfer coefficients fitted to the B data) somewhat better represented the initial Br^- concentration increase, but predicted a peak of 6 mg/L in early March 2000 that considerably exceeded the data (Fig. 6b).

The C plot had the narrowest tile drain spacing (12 m) among the three plots (Table 2). C also had the shallowest tile drains (96 cm), but with tile drain depth only slightly smaller than at B (101 cm). From the beginning, the measured drainage curve was slightly overestimated by the 2D-MIM, and more so by the 1D-MIM (Fig. 8a). Plot C, similarly as A, had a plateau-like measured Br^- BTC with gradually decreasing concentrations (Fig. 8b). The observed Br^- concentrations were closely approximated by the 2D-MIM prediction. Although the 1D-MIMforward predicted a late start of the Br^- BTC, it matched very

well the concentration level of 7 mg/L measured at the beginning of the Br^- BTC. Starting from January 2000, the 1D-MIMforward overestimated the measured Br^- concentrations. The 1D-MIM predicted an early peak of almost 15 mg/L and a secondary peak that again overestimated Br^- measurements.

Neither the 1D-MIM nor the 1D-MIMforward case (using transfer parameters obtained from plot B data) adequately predicted observations of plots A and C having different drainage geometries than B. The failure of the 1D-MIM prediction became particularly obvious by the unrealistically high Br^- peak simulated for the C plot. This failure revealed that a calibrated 1D-MIM model cannot be used to predict solute transport in tile-drained field plots, since it does not consider the tile-drain induced flow field. When we fitted α_s on the B data (1D-MIM case), the resulting α_s values for two upper layers with mainly vertical flow hardly changed (H1: $\alpha_s = 0.020 \text{ d}^{-1}$, H2:

$\alpha_s = 0.023 \text{ d}^{-1}$) and hence appeared to be close to the optimal values; only α_s of the H3 horizon was reduced from 0.075 to 0.016 d^{-1} (Table 3) to compensate for the 2D-flow field effects on the Br^- BTC. Recently, Köhne and Gerke (2005) stated the relevance of the 2D transport scheme at tile drained fields with non-equilibrium flow. Moreover, Abbaspour et al. (2001) found that multiple parameter fitting does not yield satisfactory transport predictions unless all relevant processes are described. In our study, the solute transfer coefficients in the 1D-MIM approach that were fitted to B data must be viewed as effective parameters that are specific only to the B plot. The 2D-MIM gave a more consistent description of observed Br^- transport (and water flow) at the 3 plots with different tile-drainage geometries. Hence, parameters of the 2D-MIM that were calibrated against observations from one plot could be used to adequately predict physical non-equilibrium solute transport in plots with different tile drain configurations.

4. Conclusions

The observed rapid bromide breakthrough at the tile-drained Infeld site without high initial peak was characterized as weakly preferential. The systematic comparison between 1D and 2D single- and dual-porosity model simulations suggested two major underlying transport processes. First, the tile-drain induced flow field with variable lengths of unsaturated and saturated transport pathways from the surface towards the tile drain dispersed the Br^- tracer concentrations in drain effluent. Second, physical non-equilibrium gave rise to rapid solute leaching, but large solute mass transfer into immobile regions prevented the high early solute losses typical for preferential flow.

The fact that 2D-MIM simulations were more accurate for different tile drain configurations than 1D-MIM simulations imply that the two-dimensional flow should be considered when aiming at a mechanistic description of physical non-equilibrium solute transport in tile-drained fields. The 2D-MIM simulations explained the observed Br^- concentrations level with over 60% of the applied Br^- mass being initially

transferred into immobile soil regions, and stored there throughout the drainage season.

The MIM (compared with SPM) analyses showed that even when physical non-equilibrium transport increases early mass loss, in the long run mass transfer may slow down solute leaching. In case of degradable chemicals, however, immobilization of a solute as caused by mass transfer and slow release may leave time for efficient decay of a chemical.

Acknowledgements

This work was financed by Deutsche Forschungsgemeinschaft grant no. LE 945 4-1 and promoted by the Dept. of Environmental Sciences, University of California in Riverside. The authors greatly thank the Landwirtschaftskammer Weser-Ems for providing the instrumented experimental field site, preliminary data, and technical support. Furthermore, we acknowledge Stefan Arndt for his contribution in the experimentation and data compilation. The authors sincerely appreciate the support of Dr. Schäfer from Bodentechnisches Institut Bremen des Niedersächsisches Landesamt für Bodenforschung (BTI/NLFB) for this research project.

References

- Abbasi, F., Feyen, J., van Genuchten, M.Th., 2004. Two dimensional simulations of water flow and solute transport below furrows: model calibration and validation. *J. Hydrol.* 290, 63–79.
- Abbaspour, K.C., Kohler, A., Simunek, J., Fritsch, M., Schulin, R., 2001. Application of a two-dimensional model to simulate flow and transport in a macroporous agricultural soil with tile drains. *Eur. J. Soil Sci.* 52, 433–447.
- Andreu, L., Moreno, F., Jarvis, N.J., Vachaud, G., 1994. Application of the model MACRO to water movement and salt leaching in drained and irrigated marsh soils, Marismas, Spain. *Agric. Water Manage.* 25, 71–88.
- Bear, J., 1972. *Dynamics of Fluids in Porous Media*. Elsevier, New York.
- Bouma, J., 1990. Using morphometric expressions for macropores to improve soil physical analyses of field soils. *Geoderma* 46, 3–11.
- Diez, T., Weigelt, H., 1987. *Böden unter landwirtschaftlicher Nutzung*. BLV Verlagsgesellschaft, München pp. 108–109.
- DVWK, 1996. *Ermittlung der Verdunstung von Land- und Wasserflächen*. Merkblätter zur Wasserwirtschaft, Heft 238. Wirtschafts- und Verlagsgesellschaft Gas und Wasser mbH, Bonn.
- Fipps, G., Skaggs, R.W., 1986. Drains as a boundary condition in finite elements. *Water Resour. Res.* 22, 1613–1621.

- Fortin, J., Gagnon-Bertrand, E., Vézina, L., Rompé, M., 2002. Preferential bromide and pesticide movement to tile drains under different cropping practices. *J. Environ. Qual.* 31, 1940–1952.
- Gerke, H.H., Köhne, J.M., 2004. Dual-permeability modeling of preferential bromide leaching from a tile drained glacial till agricultural field. *J. Hydrol.* 289, 239–257.
- Gerke, H.H., Van Genuchten, M.Th., 1993. A dual-porosity model for simulating the preferential movement of water and solutes in structured porous media. *Water Resour. Res.* 29, 305–319.
- Gish, T.J., Kung, K.-J.S., Perry, D.C., Posner, J., Bubenzer, G., Helling, C.S., Kladvik, E.T., Steenhuis, T.S., 2004. Impact of preferential flow at varying irrigation rates by quantifying mass flux. *J. Environ. Qual.* 33, 1033–1040.
- Haws, N.W., Rao P.S.C., Šimůnek, J., Poyer, I.C., 2005. Single-porosity and dual-porosity modeling of water flow and solute transport in subsurface-drained field using effective field-scale parameters. *J. Hydrol.* (in press) doi: 10.1016/j.hydrol.2005.03.035.
- Jardine, P.M., Jacobs, K.G., Wilson, G.V., 1993. Unsaturated transport processes in undisturbed heterogeneous porous media: I. Inorganic contaminants. *Soil Sci. Soc. Am. J.* 57, 945–953.
- Jarvis, N.J., 1994. The MACRO Model. (Vers. 3.1.) Technical description and sample simulations. Reports and Dissertations 19. Department of Soil Science. Swedish University of Agricultural Science, Uppsala, Sweden, p. 51.
- Jarvis, N.J., 1998. Modeling the impact of preferential flow on nonpoint source pollution. In: Selim, H.M., Ma, L. (Eds.), *Physical Non-equilibrium in Soils: Modeling and Application*. Ann Arbor Press, Chelsea, MI, pp. 195–221.
- Jaynes, D.B., Logsdon, S.D., Horton, R., 1995. Field method for measuring mobile/immobile water content and solute transfer rate coefficient. *Soil Sci. Soc. Am. J.* 59, 352–356.
- Jaynes, D.B., Ahmed, S.I., Kung, K.-J.S., Kanwar, R.S., 2001. Temporal Dynamics of preferential flow to subsurface drain. *Soil Sci. Soc. Am. J.* 65, 1368–1376.
- Kladvik, E.T., van Scoyoc, G.E., Monke, E.J., Oats, K.M., Pask, W., 1991. Pesticide and Nutrient movement into subsurface tile drains on a silt loam soil in Indiana. *J. Environ. Qual.* 20, 264–270.
- Köhler, A., Abbaspour, K.C., Fritsch, M., van Genuchten, M.Th., Schulin, R., 2001. Simulating unsaturated flow and transport in a macroporous soil to tile drains subject to an entrance head: model development and preliminary evaluation. *J. Hydrol.* 254, 67–81.
- Köhler, A., Abbaspour, K.C., Fritsch, M., Schulin, R., 2003. Using simple bucket models to analyze solute export to subsurface drains by preferential flow. *Vadoze Zone J.* 2, 68–75.
- Köhne, J.M., Gerke, H.H., 2005. Spatial and temporal dynamics of preferential bromide movement towards a tile drain. *Vadoze Zone J.* 4, 79–88.
- Kung, K.-J.S., Steenhuis, T.S., Kladvik, E.T., Gish, T.J., Bubenzer, G., Helling, C.S., 2000. Impact of preferential flow on the transport of adsorbing and non-adsorbing tracers. *Soil Sci. Soc. Am. J.* 64, 1290–1296.
- Kung, K.-J.S., Kladvik, E.T., Gish, T.J., Steenhuis, T.S., Bubenzer, G., Helling, C.S., 2000. Quantifying preferential flow by breakthrough of sequentially-applied tracers: silt loam soil. *Soil Sci. Soc. Am. J.* 64, 1296–1304.
- Larsson, M.H., Jarvis, N.J., 1999. A dual-porosity model to quantify macropore flow effects on nitrate leaching. *J. Environ. Qual.* 28, 1298–1307.
- Larsson, M.H., Jarvis, N.J., Torstensson, G., Kasteel, R., 1999. Quantifying the impact of preferential flow on solute transport to tile drains in a sandy field soil. *J. Hydrol.* 215, 116–134.
- Lennartz, B., Meyer-Windel, S., 1995. The role of immobile water in unsaturated substrates. *Hydrogéologie* 4, 75–83.
- Lennartz, B., Michaelsen, J., Wichtmann, W., Widmoser, P., 1999. Time variance analysis of preferential solute movement in a tile drained field site. *Soil Sci. Soc. Am. J.* 63, 39–47.
- Maraqa, M.A., Wallace, R.B., Voice, T.C., 1997. Effects of degree of water saturation on dispersivity and immobile water in sandy soil columns. *J. Contam. Hydrol.* 25, 199–218.
- Meyer-Windel, S., 1998. Transport processes of bromide and herbicides under steady-state and transient flow conditions, Schriftenreihe Institut für Wasserwirtschaft u. Landschaftsökologie der Christian-Albrechts Universität Kiel, Heft 28 p. 113.
- Mohanty, B.P., Bowman, J.M., Hendrickx, J.M.H., Šimůnek, J., van Genuchten, M.Th., 1998a. Preferential transport of nitrate to a tile drain in an intermittent-flood-irrigated field: model development and experimental evaluation. *Water Resour. Res.* 34, 1061–1076.
- Mohanty, B.P., Skaggs, T.H., van Genuchten, M.Th., 1998b. Impact of saturated hydraulic conductivity on the prediction of tile flow. *Soil Sci. Soc. Am. J.* 62, 1522–1529.
- Neuhaus, H., 1983. Nitratmobilität bei Grünlandnutzung auf gedränten tonreichen Marschböden. *Zeitschrift für Kulturtechnik und Flurbereinigung* 24, 347–357.
- Richard, T.L., Steenhuis, T.S., 1988. Tile drain sampling of preferential flow on a field scale. *J. Contam. Hydrol.* 3, 307–325.
- Richter, D., 1995. Ergebnisse methodischer Untersuchungen zur Korrektur des systematischen Meßfehlers des Hellmann-Niederschlagsmessers, Berichte des Deutschen Wetterdienstes, p. 194.
- Šimůnek, J., de Vos, J.A., 1999. Inverse optimization, calibration and validation of simulation models at the field scale. In: Feyen, J., Wiyu, K. (Eds.), *Modelling Transport Processes in Soils at Various Scales in Time and Space Proc. of Intern. Workshop of Europ. Agric. Eng. Field of Interest on Soil and Water*, Leuven, Belgium, 24–26. Wageningen Pers, Wageningen, The Netherlands, pp. 431–445.
- Šimůnek, J., Šejna, M., van Genuchten, M. Th., 1998. The HYDRUS-1D software package for simulating one-dimensional movement of water, heat, and multiply solutes in variably saturated media. Version 2.0, IGWMC-TPS-70, International Ground Water Modelling Center, Colorado School of Mines, Golden, Colorado, p. 251.
- Šimůnek, J., Šejna, M., van Genuchten, M. Th., 1999. The HYDRUS-2D software package for simulating two-dimensional movement of water, heat, and multiply solutes in variably saturated media. Version 2.0, IGWMC-TPS-53, International Ground Water Modelling Center, Colorado School of Mines, Golden, Colorado, p.202.
- Šimůnek, J., Jarvis, N.J., Van Genuchten, M.Th., Gärdenäs, A., 2003. Review and comparison of models for describing non-equilibrium and preferential flow and transport in the vadose zone. *J. Hydrol.* 272, 14–35.

- Skaggs, R.W., Skaggs, R.W., 1980. Drainmod reference report, Methods For Design And Evaluation Of Drainage-water Management Systems For Soils With High Water Tables. USDA, Soil Conservation Service, Fort Worth, TX.
- Skaggs, T.H., Kabala, Z.J., Jury, W.A., 1998. Deconvolution of a nonparametric transfer function for solute transport in soils. *J. Hydrol.* 207, 170–178.
- Southwick, L.M., Willis, G.H., Selim, H.M., 1992. Leaching of atrazine from sugarcane in southern Louisiana. *J. Agric. Food Chem.* 40, 1264–1268.
- Twitty, K., Rice, J., 2001. National Engineering Handbook Part 624, Chapter 10, Water Table Control, USDA, NRCS, 104 p.
- Utermann, J., Kladvik, E.J., Jury, W.A., 1990. Evaluating pesticide migration in tile-drained soils with a transfer function model. *J. Environ. Qual.* 19, 707–714.
- Vanderborght, J., Mallants, D., Vanclooster, M., Feyen, J., 1997. Parameter uncertainty in the mobile-immobile solute transport model. *J. Hydrol.* 190, 75–101.
- Van Genuchten, M.Th., 1980. A closed-form equation for predicting the hydraulic conductivity of unsaturated soils. *Soil Sci. Soc. Am. J.* 44, 892–898.
- Van Genuchten, M.Th., Wierenga, P.J., 1976. Mass transfer studies in sorbing porous media, I. Analytical solutions. *Soil Sci. Soc. Am. J.* 40, 473–481.
- Wendling, U., Schellin, H.G., Thomä, G., 1991. Bereitstellung von täglichen Informationen zum Wasserhaushalt des Bodens für die Zwecke der agrar-meteorologischen Beratung. *Z. Meteorologie* 41, 468–475.